Ultra-Low Emissivity Alpha-Particle Detection

Michael S. Gordon, *Member, IEEE*, Kenneth P. Rodbell, *Senior Member, IEEE*, Henry H. K. Tang, *Member, IEEE*, Paul Ronsheim, Zhengmao Zhu, Stewart E. Rauch, *Senior Member, IEEE*, Brendan D. McNally, *Member, IEEE*, and Stuart Coleman

***Abstract*—New alpha counters make accurate measurements of low emissivity samples possible. Modeling results set lower limits for measurements at sea level of silicon substrates to about $0.3\ \alpha$/khr-cm^2. Our measurements demonstrate the effect of cosmic ray shielding on the measured alpha-particle emissivity. A few atoms of radon contamination can cause elevated emissivities many days after exposure.**

***Index Terms*—Alpha particles, energy spectra, ionization detectors, low-background, radon, terrestrial neutrons.**

I. Introduction

It is well understood that the alpha-particle contribution to single-event upsets (SEUs) is crucially important. Autran *et al.* have shown in bulk SRAM memories that although both the alpha and neutron contributions to the SEU error rate have decreased with scaling, from 130 nm to 65 nm (with the alpha component decreasing faster than the terrestrial neutron component) the alpha component continues to be larger than the neutron component [1], [2]. Recently, Autran published results from testing of a 40 nm SRAM. These results showed that while the combined SEU rate is lower than that for the 65 nm SRAM, the 40 nm SRAM neutron component is larger and the alpha-particle component is smaller than the results from the 65 nm SRAM. They attribute the increase in neutron sensitivity to an increase in multicell upsets and possible new upset mechanisms. The continued reduction in the alpha-particle component has been due to a decrease in the wafer-level alpha-particle emissivity from $2.3\ \alpha$/khr-cm^2 to $0.9\ \alpha$/khr-cm^2 for the 130 nm and 40 nm technology respectively [3].

These trends observed by Autran for 130 nm and 65 nm SRAM devices have been modeled by Wrobel *et al.* using Monte Carlo methods [4]. Wrobel showed that a few tenths of a ppb of uranium in silicon could cause an SEU rate similar to that of neutrons for the 130 nm SRAM data [5].

Recently, many papers have appeared that discuss the relative importance of U and Th in bulk silicon to the alpha-particle emissivity and the alpha-particle component of the SEU rate [5]–[10]. Reference [9] discusses modeling results that show that only 76 ppt of ^{238}U and 101 ppt of ^{232}Th can give an alpha-particle emissivity from a silicon wafer of $0.4\ \alpha$/khr-cm^2. This is in part based on the measured ^{238}U/^{232}Th ratio in silicon wafers by Dyer [11]. Dyer used neutron activation analysis to measure the amount of ^{238}U and ^{232}Th in silicon wafers, and the concentrations were on the order of 20 ppt [11]. IBM also has data on ^{238}U and ^{232}Th content of silicon wafers from neutron activation studies which show levels < 7 ppt [12].

Recent work from Martinie *et al.* has shown modeling results of the alpha-particle emissivity caused by ^{238}U and ^{232}Th in bulk silicon as a function of the silicon thickness for a variety of detector threshold energies [10]. Unfortunately, the nomogram in the paper that shows the results of U and Th does not show the alpha-particle emissivity for detection thresholds <2 MeV. In any event, they show that for a silicon wafer, using a detection threshold of 2 MeV, $\sim$86 ppt of ^{238}U corresponds to an alpha-particle emissivity of $\sim\ 0.3\ \alpha$/khr-cm^2. The alpha-particle emissivity increases to $\sim\ 0.5\ \alpha$/khr-cm^2 if, in addition to the 86 ppt of ^{238}U, $\sim$200 ppt ^{232}Th is included in the bulk of the silicon.

These ppt levels of U and Th present a measurement challenge. Several variants of inductively coupled plasma mass spectrometry (ICP-MS) might be considered for detecting U or Th in Si. Vapor phase decomposition (VPD) ICP-MS is useful for measuring the contamination on the surface of a wafer, however, bulk Si dissolution coupled with high resolution magnetic sector (HR) ICP-MS was developed to determine ultratrace elemental impurities within a bulk silicon. The detection limits of HR ICP-MS for U or Th are <100 ppt [13].

In addition to the emissivity from the contamination of U and/or Th in the bulk Si wafer, one might also introduce contamination in the back end of the line (BEOL), underfill, or solder bumps which could all contribute to the alpha-particle component to the SEU error rate. For reference, an alpha-particle emissivity of $0.7\ \alpha$/khr-cm^2, corresponds to the detection of only $0.5\ \alpha$/hr for a 300 mm wafer. Measuring these low emissivities accurately is now possible using a new class of ultra-low background alpha-particle detector [14], [15]. The alpha-particle spectrum can be obtained in addition to the sample emissivity which can allow for isotope identification in the case of surface emission [15]. Accurate, direct measurements of the alpha-particle emissivity from the BEOL and from the silicon substrates is a goal is this work, so that the alpha-component to our SEU model can be verified and reduced.

This paper is organized as follows. First we review the operating principles of the ultra-low background ionization counter used in this work. Next we discuss limits to the detection of ultra-low alpha-particle emission levels. In this regard, we have

Manuscript received July 13, 2012; revised September 13, 2012 and September 17, 2012; accepted September 18, 2012. Date of current version December 11, 2012.

M. S. Gordon, K. P. Rodbell, and H. H. K. Tang are with the IBM T.J. Watson Research Center, Yorktown Heights, NY 10598 USA (e-mail: gordonm@us.ibm.com).

P. Ronsheim, Z. Zhu, and S. E. Rauch are with IBM's Semiconductor Research and Development Center, Hopewell Junction, NY 12533 USA.

B. McNally and S. Coleman are with XIA LLC, Hayward, CA 94544 USA.

Color versions of one or more of the figures in this paper are available online at http://ieeexplore.ieee.org.

Digital Object Identifier 10.1109/TNS.2012.2223234

developed a model to predict the alpha-particle production from the interaction of cosmogenic particles on silicon, and in the argon gas in the counter, and we show how these reactions generate a lower detection limit even for samples with zero-emissivity. Finally we discuss the influence of radon on the sample being measured. This can affect the first few hours or days of measurement. Another advantage of being able to measure the energy of alpha particles emitted from the sample is that we can track the time-evolution of the number of alpha particles and understand their origin.

II. Ionization Counter Operation

The alpha-particle data shown in this paper were obtained from an early commercial ionization detector (UltraLo-1800) from XIA that has a very low background count rate and the ability to measure the energy and arrival time of each alpha-particle emitted from the sample. It is a refined version of the prototype version discussed in [14] and [15]. The sample resides on the cathode and is immersed within the electric field of the counter. The anode is biased to 1000 V and contains two user-selectable segments: either a 300 mm diameter circle or a 1800 cm^2 square.

When the alpha particles ionize the argon counter gas, the electron tracks drift toward the anode and induce a steady current in the attached electronics that generates a linear rise in the pulse shape. Once the topmost (earliest) electrons in the track strike the anode, they stop contributing to the current induction process and the pulse shape transitions from a linear to a parabolic rise. This "rounding" persists until the final electrons are collected on the anode. The total risetime of the pulse (in this case, linear+parabolic) indicates how far the electrons drifted. The amount of time that the pulse is parabolic (or "round") is a measure of the vertical projection of the track orientation in the counter.

Each pulse is analyzed and an amplitude is measured which corresponds to the energy of the original alpha particle. The alpha-particle energy defines its track length in the argon, and also sets the maximum amount of roundness that the event could possibly attain. If a pulse is analyzed, and determined to be too round for its measured energy, the event is categorized as "Round". For example, a signal generated by an ionization track from a particle or fragment with a dE/dx less than that of an alpha particle is but one physical cause for the observation of a "Round" event (not an "alpha"). A discussion of the origin of these events will be given in Section III-D.

A guard ring surrounds the anode and is used to veto alpha particles emitted from the side walls. Every event is tagged with the time of arrival, and the pulse shape is fit in real time. Depending on the pulse amplitude, risetime, the shape of the anode signal, and whether an event induces a charge on the guard electrode, the event is classified as a valid alpha particle or not. A file is exported for offline analysis and contains the classification of the event, pulse amplitude, risetime, energy and arrival time.

A cross section of the counter is shown in Fig. 1. Alpha-particles emanating from the sidewall, anode (ceiling) and sample are shown symbolically as α_s, α_c and α, respectively. Another class of events known as "mid-air" is shown and

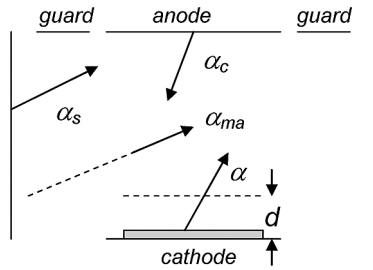

Fig. 1. Cross section of the ionization counter with different classes of events.

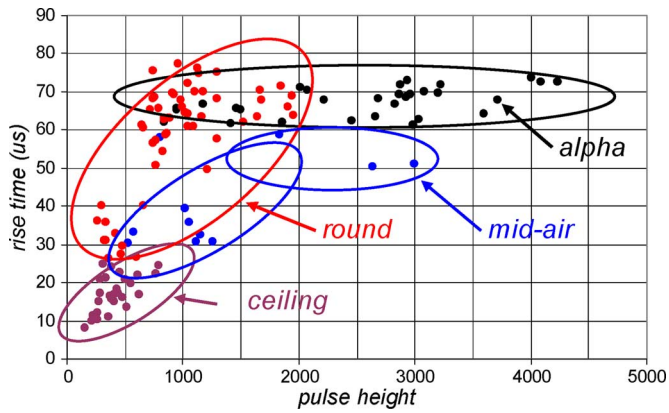

Fig. 2. Scatter plot of risetime as a function of pulse height, and the classifications, for events detected.

is labeled as α_{ma}. The mid-air events are those in which alpha particles appear above the sample surface, generating signals whose risetimes are smaller than those from alpha particles emanating from the sample. These alpha particles might be due to radon production in or on the counter materials. The radon gas may then be released and can later emit alpha particles anywhere in the counter volume. The minimum signal risetime for alpha particles coming from the sample is determined by placing a low-activity source on the sample stage. Another origin of the mid-air events might be cosmogenic particles like protons.

For samples with dimensions smaller than the sample tray, alpha particles emitted from the tray are indistinguishable from alpha particles emitted from the sample. For the work reported here, all samples used are larger than or equal to the active area of the sample tray (300 mm diameter) to eliminate any influence from the sample tray.

A scatter plot of events that have been classified is shown in Fig. 2, where the event risetime is plotted as a function of the signal pulse height (energy). This shows that round events have small amplitude, ceiling events have both small amplitude and small risetime, and mid-air events can have appreciable risetime and pulse height, but smaller risetimes than sample alpha-particle events.

III. Alpha Production Mechanisms

A. General Comments

For the proportional counters in use in large numbers by the electronics industry, the counter background (count rate in the absence of a sample) is on the order of a few counts/hr and

is controlled by the judicious choice of materials used to construct the counter. Typically the background is counted before the sample, and the background count rate is subtracted from sample count rate. Often the background is measured before and after the sample and the average count rate is subtracted from the sample count rate, or a moving average of the background count rate is used [16].

The UltraLo-1800 in use for this work has active signal rejection, as mentioned above. As such, it is expected that a sample with no alpha-particle emission would necessarily register zero alpha-particle events during a measurement without the need for background subtraction.

We have observed an alpha-particle emissivity of $\sim \ 0.3\alpha/\text{khr-cm}^2$ on several different unprocessed 300 mm wafers using several of the UltraLo-1800 counters in two of our IBM sites. As mentioned in Section I, neutron activation studies of bare silicon wafers have shown levels of ^{238}U and ^{232}Th that are $<$ 20 ppt [11], [12]. According to [9] and [10], this should yield alpha-particle emissivities of $< \ 0.1 \ \alpha/\text{khr-cm}^2$ ($<$ 2 alpha particles detected per day for a 300 mm diameter wafer). In order to help explain this discrepancy, we began a modeling effort to describe two effects that have not been considered, to our knowledge, in discussions of ultra-low alpha-particle counting.

B. $^{28}Si(n,\alpha)$ *Nuclear Reaction*

Many of the samples under investigation in our laboratory are silicon wafers with different levels of wiring, known as back-end-of-line (BEOL), which include dielectrics, aluminum, titanium, copper, tungsten and tantalum. For new technologies it is important to confirm our alpha-particle emissivity estimates based on the materials and processes used since the emissivity is an input to our SEU models. It is therefore critical to know if the baseline alpha-particle emissivity measured for bare silicon wafers is a detection threshold (in which case one could subtract this from subsequent wafer-based measurements) or if it really represents their true alpha-particle emissivity.

Several researchers have investigated neutron-induced spallation events on silicon and BEOL materials in an effort to predict or explain the neutron component of the single event upsets. For example, Wrobel *et al.* calculated the number of neutron-induced nuclear reactions on a sample of material $1 \ \text{mm}^2 \times 1 \ \text{um}$ thick, as a function of the atomic number of the sample [17]. The number of reactions increases monotonically with atomic number for the naturally-occurring elements. This model is simplistic because not all nuclear reactions lead to the emission of a particle that can cause a bit upset. Recently Uznanski *et al.* calculated the proportion of secondary ions for neutron-induced reactions on Si, including He, that could produce more than 0.5 fC of charge, which is useful for SEU calculations, but did not calculate the flux of alpha particles emitted from the Si [18].

For our application we assume all alpha particles are produced by hadronic processes. Our first model considers the effect of terrestrial neutrons, protons and pions on a 300 mm diameter silicon substrate to estimate the alpha-particle yield in the detection direction. The model estimates are based on Monte Carlo calculations done in the framework of IBM's SEMM-2 SEU simulation system [19]. They depend on three major inputs: 1) the high-energy spallation reactions of neutrons, protons and pions on silicon (20 MeV–1.5 GeV) simulated by the NUSPA code [20], [21]; 2) the measured $(\text{n}, \alpha\text{x})$ cross sections for low-energy reactions (neutron energy $<$20 MeV)[22]; and 3) the terrestrial neutron flux (1 MeV–1.5 GeV) taken from the measured data [23], [24] and the published terrestrial proton and pion flux [25].

We simulated a Si slab with a thickness of 760 μm radiated by cosmic ray particles. The basic setup is the same as in [26], involving three basic steps. In step 1, random nuclear collision points are generated in the Si slab. In step 2, at each collision point secondary particles—which typically consist of protons, neutrons, alpha particles, light ions and recoil nuclei are generated by the NUSPA code. In step 3, each of the nuclear reaction products generated in step 2 is transported in the slab using the SRIM-based particle energy-range relation [19], [27]. The transport calculation terminates when the secondary particle either reaches the slab surface, or stops in the slab interior. We are only interested in the secondary alpha particles in this work. The code is set to follow the alpha particles reaching the detector side of the slab. Their energies at this surface are computed, and to match the upper cut-off energy of the detector only those alpha particles below 10 MeV are counted.

To understand the underlying physics, let us examine the most important case, namely, alpha-particle production from neutron-induced reactions. The frequency of nuclear collisions $(\text{n} + \text{Si})$ in the slab depends on four parameters: 1) the neutron energy differential flux φ_{n}, 2) the number density ρ of the target atoms (in this case Si), 3) the thickness L of the slab, and 4) the reaction cross section σ_{R} for neutrons on Si. Here the reaction cross section refers to the inelastic collisions which produce many kinds of secondary particles. Since elastic collisions do not produce alpha particles, the elastic events are not simulated in this work. The neutron flux φ_{n} and reaction cross section σ_{R} are both strongly dependent on neutron energy. In particular, the terrestrial neutron flux is large at low energies. A plot of the terrestrial neutron flux as function of energy is shown in [23] and [24]. Neutron, proton and pion reaction cross sections are computed in [21]. Because of the rapid rise of neutron flux at low energies (below 100 MeV), one may be inclined to expect that, compared with high-energy neutrons, low-energy neutrons produce larger alpha-particle flux. The simulations show that this is not the case. There are two important factors to consider: the alpha-particle production threshold, and the multiplicity of secondary particles in the collisions. For the $\text{n} + \text{Si}$ system, the threshold of alpha-particle production is around 5 MeV [22]. That is, at neutron energy below 5 MeV, no alpha particles can be produced despite the large neutron flux. From 5 MeV up to around tens of MeVs, the incident neutrons produce some alpha particles. For incident neutrons with energies $>$50 MeV, the collisions tend to produce multiple particles. High-energy reactions tend to produce more secondary alpha particles. The above reasoning applies to proton and pion interactions as well.

The results of the model are shown in Table I, and suggest that the neutron-induced reaction contributes about 90% to the total from the three reactions, and at sea level, in NYC, these reactions can produce an alpha-particle emissivity of

TABLE I
ALPHA-PARTICLE EMISSIVITY (α/khr-cm^2) FROM NUCLEAR REACTIONS FROM NEUTRONS, PROTONS AND PIONS ON A Si SUBSTRATE AND 3 cm OF ARGON GAS AT STP

Incident Particle	Si	Ar
Neutron	0.108	0.194
Proton	0.011	0.022
Pion	0.001	0.002
Total	0.120	0.218

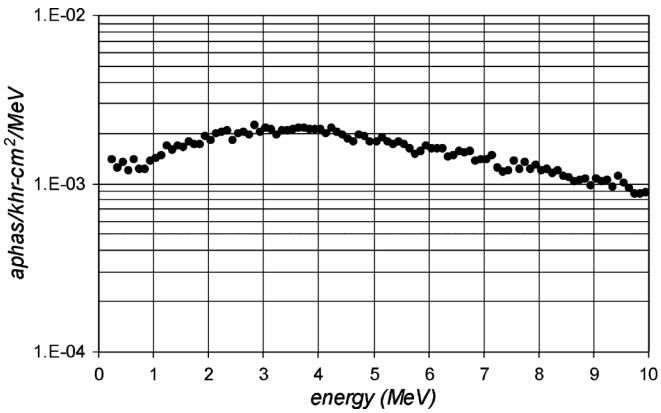

Fig. 3. Differential alpha-particle emissivity from model.

$0.12\ \alpha$/khr-cm^2. This amounts to about 1/2 of the lowest emissivity we have measured to date. This emissivity will scale with the flux of the incident particles (e.g., higher emissivity at higher elevation). Fig. 3 shows the differential emissivity (α/khr-cm^2/MeV) as a function of the alpha-particle energy from this reaction.

C. $^{40}Ar(n,\alpha)$ Nuclear Reaction

Nuclear reactions from the passage of terrestrial neutrons, protons and pions interacting with the argon counter gas can also produce alpha particles which can be detected in the counter volume. Unlike the inelastic reactions in the bulk silicon, (previous section), where some of the alpha particles are produced in the "wrong" direction, and many alpha particles are attenuated in number and in their energy by the bulk silicon above, all alpha particles created in the argon gas are eligible to be counted, even those traveling away from the active counter volume.

The calculations show a significant alpha-particle flux from neutron-argon reactions. It may seem paradoxical given the fact that the atomic number density of argon is much smaller than silicon; however, there are several contributing factors. The neutron-argon reaction cross section is larger than that of silicon and the argon gas is thicker than the silicon slab. The most important reason is that the stopping power of the alpha particles in argon gas is negligible.

Alpha particles created from the interactions within the argon gas near the anode and side walls of the counter are summarily rejected, as discussed above, based on either their pulse height, risetime, or charge induced on the guard ring. Alpha particles produced in the middle of the counter are rejected based primarily on their anode signal risetimes (classified as "mid-air" events).

One parameter required in the model is the effective "thickness" of the argon gas since the number of nuclear reactions depends on the number of target argon nuclei. We experimentally determined the gas thickness by placing a low-activity ^{230}Th source on insulating cylinders (to minimize distortion of the electric field within the counter) at a variety of distances d (see Fig. 1) above the sample tray. At distances greater than 3 cm, alpha particles from the ^{230}Th source were classified as "mid-air" events since the majority of the events had risetimes less than the 60 μs threshold established by placing the same source on the sample tray. However, for distances d $<$3 cm, more than 85% of the alpha particles emitted from the ^{230}Th source were classified as "alpha particles".

The results of this model are also shown in Table I. As with the reactions on silicon (Section III-B), the effect of the neutrons is about 90% of the total. The total alpha-particle emissivity from the reactions on the silicon substrate and in the argon gas is $0.34\ \alpha$/khr-cm^2. *This means that at sea level, in NYC, in a lightly-shielded laboratory, one would not expect to observe an emissivity less than* 0.34α/khr-cm^2, *on a blank silicon wafer (with no contamination)*. Of course, the neutron flux is larger at higher elevations, and lower in shielded laboratories (e.g., in the lower levels of buildings).

The commercially available proportional gas counters in use, world-wide, typically use either P-10 or P-5 (90% argon-10% methane, or 95% argon-5% methane, respectively). The active counter volume is smaller than that in the ionization counter, so the effect of the interactions on the argon gas would necessarily be smaller than the calculations shown above for the ionization detector.

D. Experimental Data

Recently McNally discussed the results of alpha-particle emissivity measurements using a "traveling detector" [28]. The alpha-particle emissivity of a silicon substrate was measured using a beta prototype of XIA's ionization detector for the same 48 hours measurement time, in an identical configuration at several locations, including two underground sites, and one high in the French Alps.[1] The data shown in Fig. 4 present a clear altitude-dependence, and once underground, the alpha-particle yield apparently saturates with increasing depth. The inset shows data from two locations at sea-level, with one being underground. These trends are consistent, qualitatively, with our model calculations: *that the alpha-particle emission scales with the neutron flux*. The alphas observed during measurements at the underground sites are understood to be due to ^{220}Rn production from the internal components of the prototype instrument used during the experiment.

For this work, we measured the alpha-particle emissivity of a blank 300 mm wafer using the UltraLo-1800 detector in two locations *in the same building*, at the IBM TJ Watson Research Center. The first location was in the basement which houses the 3MV tandem Van de Graaff accelerator, used for SEU and materials analysis studies. The second location was on the second

[1]LSM: http://www-lsm.in2p3.fr/, Soudan: http://www.soudan.umn.edu/, ASTEP: http://www-lsm.in2p3.fr/

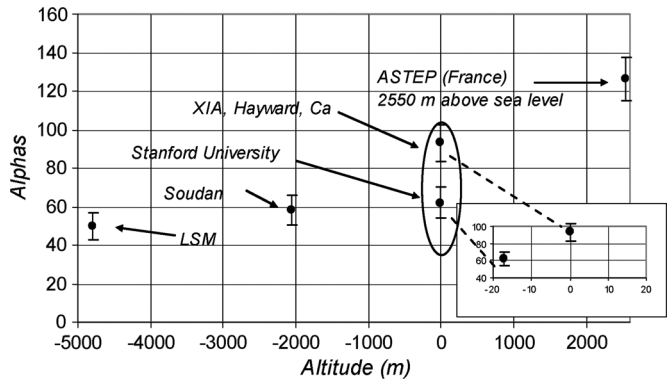

Fig. 4. The number of alpha particles detected in 48 hrs as a function of altitude, from [28]. The "altitude" for the underground sites, is actually the water-equivalent depth.

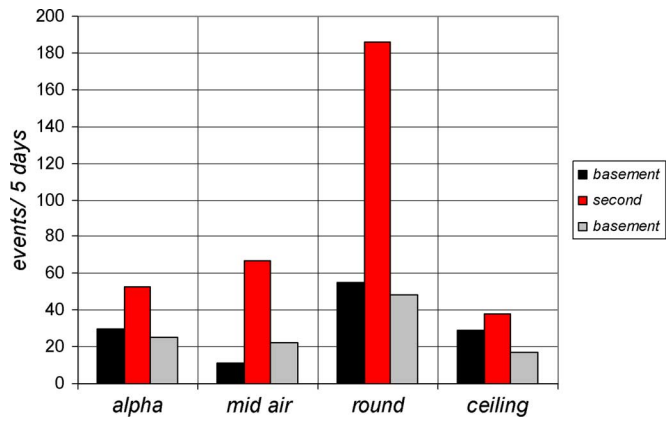

Fig. 5. Number of events for the two measurement locations.

TABLE II
THE NUMBER OF ALPHA PARTICLES, MID-AIR EVENTS, ROUND EVENTS, AND CEILING EVENTS FOR THE TWO DIFFERENT DETECTOR LOCATIONS

	Alpha	Mid-air	Round	Ceiling
Basement	30	11	55	29
2nd floor	53	67	186	38
Basement	25	22	48	27
Ratio	1.9	4.1	3.6	1.4

floor, in the corner of the building, where the detector was surrounded by two large plate-glass windows. To eliminate any effects of radon (see Section IV), we took data for 10 days or more in each location; and in the following analysis, we show and discuss the data from the last 5 days of each measurement. Additionally, the UltraLo-1800 was brought back to the basement location and the counting was repeated.

Fig. 5 shows the data for this experiment: the number of detected alpha particles, as well as events classified as "mid-air", "round" and "ceiling" for the three 5-day periods (basement, second floor and basement). For reference, the 25 alpha particles detected on the last 5-day basement run amounted to an alpha-particle emissivity of $0.35 + / - 0.06\ \alpha$/khr-cm^2. The data are summarized in Table II. Clearly there were more events of all types in the second-floor location compared to the basement location.

To estimate the effect of the building materials on the shielding of the neutron flux for the two measurement locations, we used a portable neutron detector, an ASP2E monitor from Thermo Fisher Scientific attached to a 9″ polyethylene REM ball. The 9″ polyethylene sphere allows for the detection of neutrons from thermal energies to ∼10 MeV [29]. Although the true terrestrial neutron energy distribution extends to many 10's of GeV [23], [24] this neutron monitor gives us an idea about the attenuation of the neutron flux in the building materials and earth. We observed about a 2X flux difference between the two locations. The ratio of the number of alpha-particle events, from the second floor to the basement, shown in the second column of Table II is consistent with this ratio of neutron flux. We expected to see about this 2X difference in the other classes of detected particles, but we observed ∼4X for the mid-air and round events. This increase might be due to the increased attenuation of lightly-ionizing protons compared to neutrons between the second floor and the basement locations.

In order to estimate the absolute value of the shielding of the building materials to estimate the flux loss from the terrestrial flux used in the models (see Sections III-B and III-C), we examined the building structure on the second floor and the basement where the experiments were performed. We consulted the architectural drawings for the IBM T.J. Watson Research center to determine what building materials were used above the area where the experiments were performed. For the second floor location, there was a 4.5″ concrete slab above, on the roof, and roofing materials The basement location was actually underground, just outside the perimeter of the building, with 22″ of dirt and 6″ of concrete above. For neutrons with non-normal angles of incidence, additional shielding would be provided by the concrete slabs on the first and second floors, and from the roof, to one side.

There are several references in the literature concerning the attenuation of neutrons of various energies as a function of concrete thickness [24], [30]–[32]. In [24], the attenuation of neutrons with energies >10 MeV is given by

$$\phi = \phi_0 \exp(-x/0.37) \tag{1}$$

where ϕ_0 and ϕ are the initial and final flux, respectively, and x is the thickness of the concrete in m. For the 4.5″ (0.11 m) of concrete (1) gives an attenuation of ∼26%, The attenuation values given in [32] are based on Monte Carlo simulations using GEANT4 and computed for low energy incident neutrons (0–20 MeV), and both neutrons with energies >20 MeV and >100 MeV. Using table 20 in [32], the attenuation for neutrons with energy >20 MeV through the 4.5″ concrete slab is about 13%. Similarly, [30] and [31] show minimal neutron attenuation for 0.11 m of concrete. Therefore, the high-energy portion of the neutron flux for the second floor measurement is nearly identical to outdoors (for which the model results in Sections III-B and III-C were based).

Finally, we consulted with Paul Goldhagen who collaborated with the IBM authors on our terrestrial neutron measurement paper [23]. At the time the original neutron measurements were made, the spectrometer was also placed in the same basement laboratory where the XIA UltraLo-1800 data were taken (see

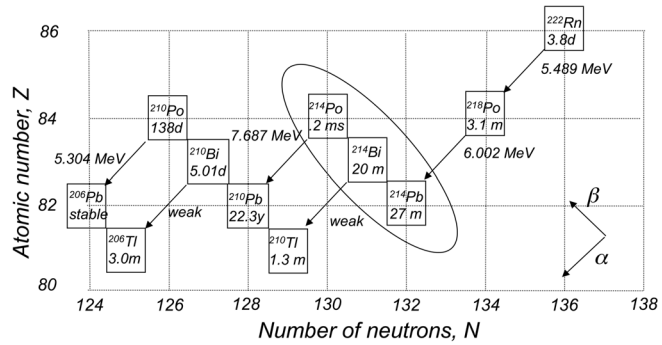

Fig. 6. The decay scheme of $^{222}\mathrm{Rn}$, from the decay of $^{238}\mathrm{U}$, which shows the isotopes from the α and β-decays, the 1/2-lives, and the alpha-particle energies.

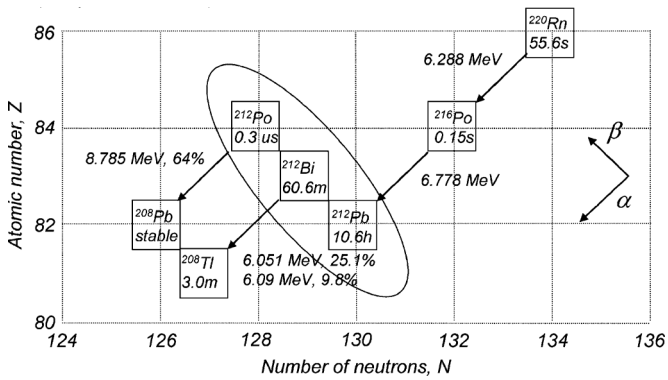

Fig. 7. The decay scheme of $^{222}\mathrm{Rn}$, from the decay of $^{232}\mathrm{Th}$, which shows the isotopes from the α and β-decay, the 1/2-lives, and the alpha-particle energies.

Section III-D). The neutron count rate ratio between the data obtained on the roof-top and the basement laboratory, for high-energy neutrons was ~2.6–4X (depending on what energy range was considered, the larger attenuation going with the higher-energy neutrons). Assuming roughly 20% attenuation between roof-top and the second floor (see the earlier discussion), leads to 2–3X reduction in neutron flux between the second floor and the basement location [33].

IV. Radon Issues

A. Isotopes, 1/2-Lives, and Alpha-Particle Energies

There are two isotopes of radon, which are commonly discussed in the literature, $^{220}\mathrm{Rn}$ (also known colloquially as "Thoron"), from the decay of $^{232}\mathrm{Th}$, and $^{222}\mathrm{Rn}$ from the decay of $^{238}\mathrm{U}$. Figs. 6 and 7 show the decay schemes, alpha-particle energies, and 1/2-lives of the daughters of $^{222}\mathrm{Rn}$ and $^{220}\mathrm{Rn}$, respectively [34].

Radon is a gas and can permeate through materials before emitting an alpha particle. The radon daughters are typically charged [35] and can attach to dust or objects charged with static electricity. This "plating out" of the radon daughters onto the surface of a sample leads to elevated alpha-particle emissivity measurements during the beginning of a measurement, after a sample is introduced into an alpha-particle counter.

Because the two isotopes of radon and their progeny come from the decay of $^{232}\mathrm{Th}$ and $^{238}\mathrm{U}$, we expect to see evidence of them from $^{232}\mathrm{Th}$ and $^{238}\mathrm{U}$ contamination, whether within the sample, in the silicon substrate, or in the counter components.

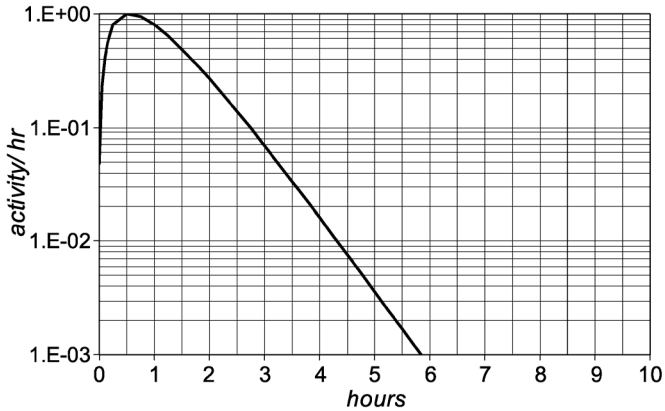

Fig. 8. The alpha-particle activity as a function of time of $^{214}\mathrm{Po}$ from applying the Bateman equation.

Because of the material above the escaping alpha particles, the energy of the alpha particles emitted from within a bulk sample will necessarily be lower than that observed from the plate out on the sample surface.

The half-lives of $^{220}\mathrm{Rn}$ and $^{222}\mathrm{Rn}$ are ~1 min and 3.8 days, respectively. The half-lives of the daughter isotopes are more important than those of the parent isotopes since: 1) the radon itself does not get attached to the sample; and 2) the daughters control the rate of alpha particles observed during the initial hours, or days (as we will show) after the sample is put into the counter.

As shown in the tilted oval in Fig. 6, within the decay chain of $^{222}\mathrm{Rn}$ is a smaller decay chain that starts with $^{214}\mathrm{Pb}$ ($\mathrm{T}_{1/2} = 26.8$ min) which β-decays to $^{214}\mathrm{Bi}$ ($\mathrm{T}_{1/2} = 19.8$ min.) and finally β-decays to $^{214}\mathrm{Po}$ (which emits an alpha particle at 7.7 MeV). The Bateman solution can be used to calculate the effective 1/2-life of any chain of radioactive decays [36]. Applying this solution to the alpha-particle emission from $^{214}\mathrm{Po}$ we show in Fig. 8 that it takes about 4.5 hours for the activity of the 7.7 MeV alpha particles to be reduced to ~0.01 of their maximum value. For this reason, due to the introduction of radon when samples are placed into alpha-particle counters, or when the sample is exposed to radon in storage, it is typical to discard at least the first four hours of data after the introduction of a sample [16]. We have found that this component is nearly always present, probably because of the long 1/2-life of $^{222}\mathrm{Rn}$.

Another important decay chain occurs within the decay of $^{220}\mathrm{Rn}$, as shown in the tilted oval in Fig. 7. It starts with $^{212}\mathrm{Pb}$ ($\mathrm{T}_{1/2} = 10.6$ hr), which β-decays to $^{212}\mathrm{Bi}$, ($\mathrm{T}_{1/2} = 60.6$ min) which then β-decays to $^{212}\mathrm{Po}$ ($\mathrm{T}_{1/2} = 0.3$ μsec). The $^{212}\mathrm{Bi}$ and $^{212}\mathrm{Po}$ daughters emit alpha particles, nearly simultaneously, at 6.1 and 8.8 MeV, respectively. As we will show, this can cause elevated alpha-particle activity for several days due to the long half-life of $^{212}\mathrm{Pb}$.

The $^{210}\mathrm{Pb} \rightarrow {}^{210}\mathrm{Po}$ decay chain is also within the decay chain of $^{222}\mathrm{Rn}$ as shown in Fig. 6. $^{210}\mathrm{Pb}$ ($\mathrm{T}_{1/2} = 22$ years) β-decays to $^{210}\mathrm{Bi}$ ($\mathrm{T}_{1/2}$ 60.6 min) which then β-decays again to $^{210}\mathrm{Po}$ ($\mathrm{T}_{1/2} = 138$ days) which is an alpha-particle emitter at 5.3 MeV. The Bateman solution applied to this decay chain produces the alpha-particle yield as a function of time shown in Fig. 9. The alpha-particle yield increases with time until it

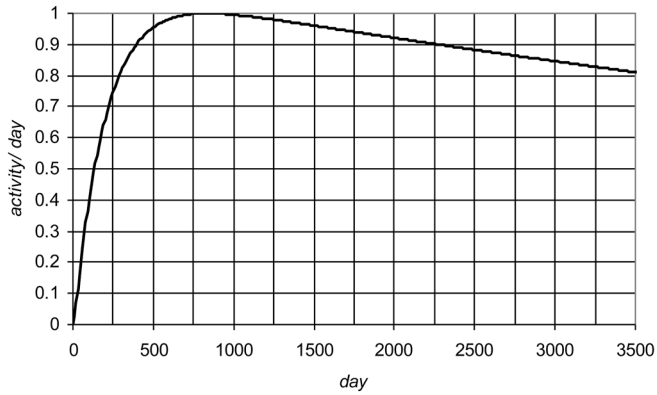

Fig. 9. The alpha-particle activity as a function of time for ^{210}Po.

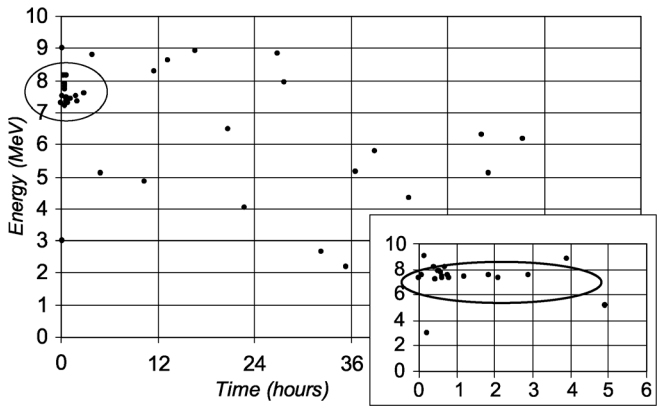

Fig. 10. The alpha-particle energy as a function of time, for a sample stored in dry nitrogen.

reaches secular equilibrium in a little over 2 years, then decays with the 22-year half-life of ^{210}Pb. The fact that the alpha-particle yield increases initially comes as a surprise to many people and for this reason it is important to make several alpha-particle measurements of Pb-based samples and project the results to secular equilibrium. We have found that electroplating can "reset the clock", which can cause the alpha-particle activity of samples to follow the distribution shown in Fig. 9 [15].

B. Experimental Evidence of Radon Plate-Out

As we will demonstrate, several factors affect the alpha-particle counting rate during the first few hours or days, such as: sample preparation; storage conditions; and the length of time a counter is open to allow for a sample to be introduced. A two-dimensional scatter plot showing the alpha-particle energy as a function of time can show the presence and decay activity of alpha particles from different isotopes of radon, as described above.

Fig. 10 shows the alpha-particle energy as a function of time, after a 45 min purge, for a sample that was stored in a dry-nitrogen environment. The inset shows the time evolution of the $\sim$7.7 MeV alpha particles from ^{214}Po over the first few hours as expected.

To demonstrate the influence of radon plate out, we exposed the same sample that was used to obtain the data in Fig. 10 to air, next to the UltraLo-1800, for a 24-hour period. The alpha-

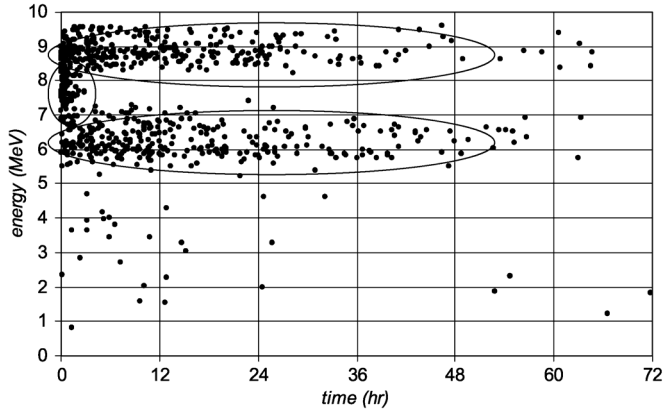

Fig. 11. The alpha-particle energy as a function of time for the same sample shown in Fig. 10, but exposed to air for 24 hours.

TABLE III
STORAGE, EXPOSURE, AND MEASUREMENT CONDITIONS

Storage condition	Exposure	Measurement
Dry Nitrogen	days	None
Air	1 hour	120 hours
Air	2.5 hours	120 hours
Pillbox	5 hours	120 hours
Air	5 hours	120 hours

particle energy plotted as a function of detection time, for this sample, is shown in Fig. 11. Three groups of alpha particles are shown by the ovals in the figure. The group near 7.7 MeV (from ^{214}Po) dies off after a few hours, as described above. The other groups, near 8.8 MeV and 6 MeV take *at least 2 days* to be reduced to background. This is a long time considering the time required to obtain a statistically accurate measurement result for samples with such low activity.

What we have observed so far, from measuring many samples, is that the 7.7 MeV alpha particles from ^{214}Po, coming from the plate out of the daughters of ^{222}Rn tend to be the only Rn daughters of importance for samples stored in dry nitrogen environments. In contrast, for samples exposed to air, *for any length of time*, 8.8 MeV and 6.1 MeV alpha particles will be observed from the decay of ^{212}Pb in the ^{220}Rn chain, in addition to the 7.7 MeV alpha-particles previously mentioned from ^{214}Po.

As a final example of the effect that a sample's storage has on the initial count rate, we took a different sample and alternately exposed it to air for different times and measured the alpha-particle yield in the UltraLo-1800. Table III describes the storage and measurement cycles.

Fig. 12 shows a histogram of the alpha particles detected in eight, 8-hour bins for each of the four exposure conditions. There is a dramatic difference between the number of alpha-particle events in the first several time bins when the sample is stored in the pillbox for 5 hours, compared to being exposed to open air in the laboratory for the same period of time.

The experiments which demonstrated the effects of radon, shown in Figs. 10–12, were performed in the basement laboratory at the IBM T.J. Watson Research Center. We used a Durridge model RAD7 radon detector to survey the radon in the

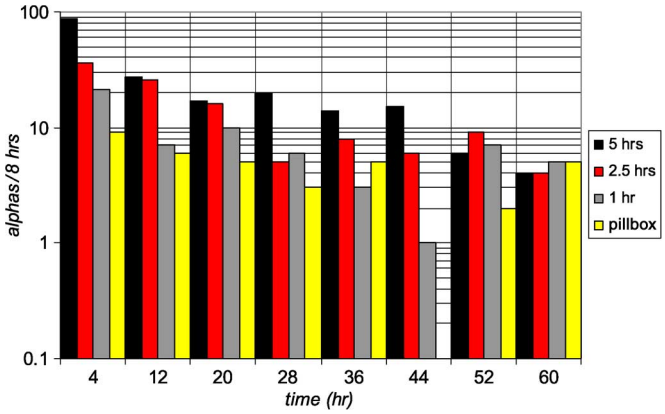

Fig. 12. The number of detected alpha particles in 8-hour bins for the same sample following different amount of time exposed to air.

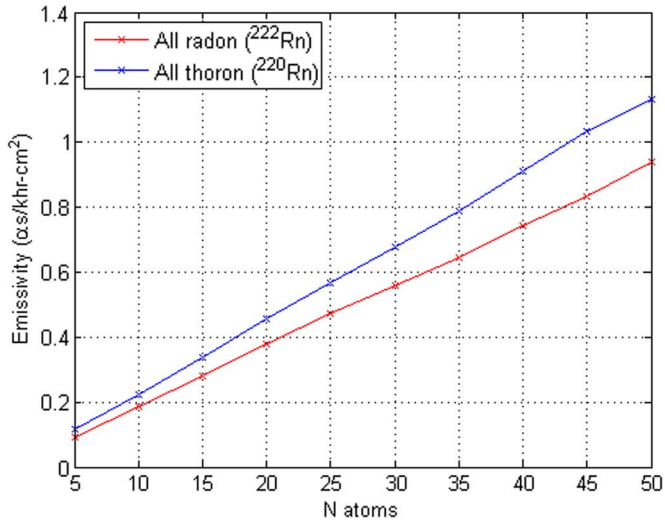

Fig. 13. Calculated emissivities for $^{222}\mathrm{Rn}$ and $^{222}\mathrm{Rn}$ as a function of number of atoms.

area where the samples were exposed to the ambient air [37]. The air was sampled for 48 one-hour periods at two locations in the laboratory. The average levels measured were $\sim 4\ \mathrm{Bq/m^3}$, or ~0.1 pCi/L. We had expected a much larger level of radon since the lab is in the basement, however it must have been low due to large number of air exchanges due to the heating and ventilation system. We want to stress that this measured radon level is about 40X lower than the EPA action limit of 4 pCi/L where it recommends remediation [38] and is a very low level.

We infer from these results that the amount of radon plated out onto the surface of samples depends on the total volume of air above the sample, to which it is exposed. Having the sample in the pillbox reduces the volume of air, even though the pillbox is not hermetically sealed. Over a long enough time, the radon plate-out would have increased due to radon permeating into the plastic pillbox, although still far less than if the pillbox was not present. The take-away from this, is that if the sample has to be exposed to air, it should be for as short of a time as possible.

The lingering effect of the radon daughters can occur when a high-activity $^{232}\mathrm{Th}$ calibration source is left in the counter for short time, or a low-activity sample for an extended period of time.

C. Radon Plate-Out Modeling

As we have seen, even trace amounts of radon exposure can lead to an appreciable amount of activity during the early stages of a measurement. To illustrate this, from a modeling standpoint, we looked into how many atoms of either $^{220}\mathrm{Rn}$ or $^{222}\mathrm{Rn}$, decaying near the surface of a 300 mm diameter sample (with no activity), with all of the progeny ending up on the sample surface, would be responsible for producing measurable alpha-particle activity on the sample. A Monte Carlo simulation was set up to determine when the decays occur, and whether the alpha-articles were emitted into 2π for a 24 hour measurement period (after a 45 min exemption period, to simulate the purge time). The results, shown in Fig. 13 indicate that only a handful of atoms are required to produce measurable and substantial emissivities. In fact, only about a dozen atoms of either $^{222}\mathrm{Rn}$ or $^{220}\mathrm{Rn}$ are needed to produce alpha-particle emissivities of $\sim 0.3\ \alpha/\mathrm{khr\text{-}cm^2}$.

V. Conclusions

The measured levels of U and Th in the literature and from IBM measurements, on bare silicon wafers using neutron activation analysis, are <20 ppt. Based on those data and Martinie's model [10], we expect the alpha-particle emissivity to be $\sim 0.1\ \alpha/\mathrm{khr\text{-}cm^2}$, yet we observed $\sim 0.3\ \alpha/\mathrm{khr\text{-}cm^2}$. In this work we investigated two sources that could contribute at this level.

First, we developed a model where cosmogenic neutrons, protons and pions interacted with silicon atoms in bulk silicon wafers, and in the argon gas within the UltraLo-1800 and produced appreciable alpha-particle emissivities. Monte Carlo methods were used to track the alpha particles in a geometry consistent with the instrument. The results of the model suggest that the neutrons are responsible for ~90% of the alpha particles generated. The alpha-particle emissivity, outdoors, in NYC, is $\sim 0.34\ \alpha/\mathrm{khr\text{-}cm^2}$, and is comparable to the emissivity we have measured for bare silicon wafers in the basement within the IBM T.J. Watson Research Center.

Second, we examined the effects of radon contaminants, which we found were significant, even at very low concentration levels of ~0.1 pCi/L. We presented some data in a two-dimensional scatter plot of alpha-particle energy vs. time, after a 45 min purge cycle, for samples stored under different conditions where they would be exposed to different amounts of laboratory air. The data clearly show 7.7 MeV alpha particles from the decay of $^{214}\mathrm{Po}$, which dies off in less than 4 hours. Alpha particles from the decays of $^{212}\mathrm{Po}$ and $^{212}\mathrm{Bi}$, however, at 8.8 MeV and 6.1 MeV, respectively, can take several days to die off due the 10.6 hour 1/2-life of the parent, $^{212}\mathrm{Pb}$. We showed that this effect could be greatly reduced by storing the sample in a pillbox, which limited the amount of laboratory air it was exposed to. Exposure to air should be kept at a minimum, including the time between manufacturing and arrival at the measurement laboratory. If these times are large, samples should be kept in closed containers, preferably hermetically sealed in an inert gas.

A Monte Carlo model of radon plate-out on a 300 mm diameter surface showed that only a dozen radon atoms are required to produce an alpha-particle emissivity of a few tenths of an alpha particle/khr-cm^2.

Lastly, we propose to the industry that we adopt the use of emissivity in units of α/khr-cm^2, rather than the older α/hr – cm^2—since the use of α/khr-cm^2 seems more appropriate for ultra-low emissivity samples. This will eliminate typing three zeros all of the time.

ACKNOWLEDGMENT

The authors would like to thank the following colleagues at IBM: C. Murray, T. Ning, P. Oldiges, L. Wissel, and G. Massey and with W. Warburton from XIA for many fruitful discussions.

REFERENCES

[1] J. L. Autran, P. Roche, S. Sauze, G. Gasiot, D. Munteanu, P. Loaiza, M. Zampaolo, and J. Borel, "Altitide and underground real-time SER characterization of CMOS 65 nm SRAM," *IEEE Trans. Nucl. Sci.*, vol. 56, no. 4, pp. 2258–2266, Aug. 2009.

[2] J. L. Autran, D. Munteanu, P. Roche, G. Gasiot, S. Martinie, S. Uznanski, S. Sauze, S. Semikh, E. Yakushev, S. Rozov, P. Loaiza, F. Warot, and M. Zampaolo, "Soft-errors induced by terrestrial neutrons and natural alpha-particle emitters in advanced memory circuits at ground level," *Microcircuits Reliab.*, vol. 50, pp. 1822–1831, 2010.

[3] J. L. Autran, S. Serre, D. Munteanu, S. Martinie, S. Semikh, and S. Sauze, in *Proc. 2012 Int. Reliability Physics Symp.*, pp. 3C.5.1–3C.5.9.

[4] F. Wrobel, F. Saigne, M. Gedion, J. Gasiot, and R. D. Schrimpf, "Radioactive nuclei induced soft errors at ground level," *IEEE Trans. Nucl. Sci.*, vol. 56, no. 6, pp. 3437–3441, Dec. 2009.

[5] F. Wrobel, J. Gasiot, and F. Saigne, "Hafnium and Uranium contributions to soft error rate at ground level," *IEEE Trans. Nucl Sci.*, vol. 55, no. 6, pp. 3141–3145, Dec. 2008.

[6] F. Wrobel, G. Gasiot, F. Saigne, and A. D. Touboul, "Effects of atmospheric neutrons and natural contamination on advanced microelectronics memories," *Appl. Phys. Lett.*, vol. 93, pp. 064105-1–064105-3, 2008.

[7] F. Wrobel, F. Saigne, M. Gedion, J. Gasiot, and R. D. Schrimpf, "Radioactive nuclei induced soft errors at ground level," *IEEE Trans. Nucl. Sci.*, vol. 56, no. 6, pp. 3437–3441, Dec. 2009.

[8] M. Gedion, F. Wrobel, F. Saigne, and R. D. Schrimpf, "Monte Carlo simulations to evaluate the contribution of Si bulk, interconnects, and packaging to alpha-soft error rates in advanced technologies," *IEEE Trans. Nucl. Sci.*, vol. 57, no. 6, pp. 3121–3126, Dec. 2010.

[9] M. Gedion, F. Wrobel, F. Saigne, and R. F. Schrimpf, "Uranium and thorium contribution to soft error rate in advanced technologies," *IEEE Trans. Nucl. Sci.*, vol. 58, no. 3, pp. 1098–1103, Jun. 2011.

[10] S. Martinie, J. L. Autran, D. Munteanu, F. Wrobel, M. Gedion, and F. Saigne, "Analytical modeling of alpha-particle emission rate at wafer-level," *IEEE Trans. Nucl. Sci.*, vol. 58, no. 6, pp. 2798–2803, Dec. 2011.

[11] F. F. Dyer, J. F. Emery, K. J. Northcutt, and R. M. Scott, "Determination of Uranium and Thorium in semiconductor memory materials by high fluence neutron activation analysis," *J. Radioanal. Chem.*, vol. 72, no. 1–2, pp. 53–67, 1982.

[12] G. Pfeiffer, Private Communication, IBM, Jan. 20, 2012.

[13] F. Li Balazs, *Private Communication.* Sep. 12, 2012.

[14] M. S. Gordon, D. F. Heidel, K. P. Rodbell, B. Dwyer-McNally, and W. K. Warburton, "An evaluation of an ultralow background alpha-particle detector," *IEEE Trans. Nucl. Sci.*, vol. 56, no. 6, pp. 3381–3386, Dec. 2009.

[15] M. S. Gordon, K. P. Rodbell, D. F. Heidel, C. E. Murray, H. H. K. Tang, B. Dwyer-McNally, and W. K. Warburton, "Alpha-particle emission energy spectrum from material used for solder bumps," *IEEE Trans. Nucl. Sci.*, vol. 57, no. 6, pp. 3251–3256, Dec. 2010.

[16] [Online]. Available: /http://www.jedec.org/standards-documents.results.jesd221.

[17] F. Wrobel, J. M. Palau, M. C. Calvert, and H. Duarte, "Incidence of multi-particle events on soft error rates caused by n-Si nuclear reactions," *IEEE Trans. Nucl. Sci.*, vol. 47, no. 6, pp. 2580–2585, Dec. 2000.

[18] S. Uznanski, G. Gasiot, P. Roche, S. Semikh, and J. L. Autran, "Combining GEANT4 and TIARA for neutron soft error-rate prediction of 65 nm flip-flops," *IEEE Trans. Nucl. Sci.*, vol. 58, no. 6, pp. 2599–2606, Dec. 2011.

[19] H. H. K. Tang, "SEMM-2: A new generation of single-event-effect modeling tools," *IBM J. Res. Dev.*, vol. 52, no. 3, pp. 233–244, 2008.

[20] H. H. K. Tang, G. R. Srinivasan, and N. Azziz, "Cascade statistical model for nucleon-induced reactions on light nuclei in the energy range 50 MeV–1 GeV," *Phys. Rev. C*, vol. 42, no. 4, pp. 1598–1622, 1990.

[21] H. H. K. Tang, "Nuclear physics of cosmic ray interaction with semiconductor materials—Particle-induced soft errors from a physicist's perspective," *IBM J. Res. Dev.*, vol. 40, no. 1, pp. 91–108, 1996.

[22] F. B. Bateman, R. C. Haight, M. B. Chadwick, S. M. Sterbenz, S. M. Grimes, and H. Vonach, "Light charged-particle production from neutron bombardment of silicon up to 60 MeV: Role of level densities and isospin," *Phys. Rev.*, vol. C60, p. 064609, 1999.

[23] M. S. Gordon, P. Goldhagen, K. P. Rodbell, T. H. Zabel, H. H. K. Tang, J. M. Clem, and P. Bailey, "Measurement of the flux and energy spectrum of cosmic-ray neutrons on the ground," *IEEE Trans. Nucl. Sci.*, vol. 51, no. 6, pp. 3427–3434, Dec. 2004.

[24] [Online]. Available: http://www.jedec.org/standards-documents/results/jesd89a.

[25] E. Ibe, T. Toba, K. Shimbo, and H. Taniguchi, "Fault-based reliable design-on-upper-bound of electronic systems for terrestrial radiation including muons, electrons, protons and low energy neutrons," presented at the 18th Int. On-Line Testing Symp., Sitges, Spain, Jun. 27–29, 2012, 3.2.

[26] N. Azziz, H. H. K. Tang, and G. R. Srinivasan, "A microscopic model of energy deposition in silicon slabs exposed to high-energy protons," *J. App. Phys.*, vol. 62, no. 2, pp. 414–418, 1987.

[27] [Online]. Available: http://www.SRIM.org.

[28] B. McNally, "Recent advances in alpha counting technology," in *Proc. 3rd Annu. IEEE—Santa Clara Valley Soft Error Rate (SER) Workshop*, Oct. 27, 2011. [Online]. Available: http://ewh.ieee.org/soc/cpmt/presentations/cpmt1110w-9.pdf.

[29] [Online]. Available: http://www.thermo.com/eThermo/CMA/PDFs/Product/productPDF_25293.pdf.

[30] J. D. Dirk, M. E. Nelson, J. F. Ziegler, A. Thompson, and T. H. Zabel, "Terrestrial thermal neutrons," *IEEE Trans. Nucl. Sci.*, vol. 50, no. 6, pp. 2060–2064, Dec. 2003.

[31] J. F. Ziegler, "Terrestrial cosmic rays," *IBM J. Res. Dev.*, vol. 40, no. 1, pp. 19–39, Jan. 1996.

[32] E. Aguayo, A. S. Ankney, T. J. Berguson, R. T. Kouzes, J. L. Orrell, and M. D. Troy, Cosmic ray interactions in shielding materials PNNL-20693, Jul. 2011, pp. 1–67.

[33] P. Goldhagen, *Private Communication.* Sep. 12, 2012.

[34] Chart of the Nuclides. [Online]. Available: http//www.nndc.bnl.gov/chart/.

[35] S. Burgos, J. Forbes, C. Ghag, M. Gold, V. A. Kudryavtsev, T. B. Lawson, D. Loomba, P. Majewski, D. Muna, A. StJ. Murphy, G. G. Nicklin, S. M. Paling, A. Petkov, S. J. S. Plank, M. Robinsonm, N. Sanghi, N. J. T. Smith, D. P. Snowden-Ifft, N. J. C. Spooner, T. J. Sumner, J. Turk, and E. Tziaferi, "Track reconstruction and performance of DRIFT directional dark matter detectors using alpha particles," *Nucl. Instrum. Meth. A*, vol. 584, pp. 114–128, 2008.

[36] H. Bateman, "Solution of a system of differential equations occurring in the theory of radio-active transformations," *Proc. Cambridge Phil. Soc. IS*, vol. 423, 1910.

[37] [Online]. Available: http://www.durridge.com/products_rad7.shtml.

[38] [Online]. Available: http://www.epa.gov/radon/pubs/citguide.html.